Experimental test of the diffusion approximation for multiply scattered sound

J. H. Page,[1] H. P. Schriemer,[1] A. E. Bailey,[2,3] and D. A. Weitz[3]
[1]*Department of Physics, University of Manitoba, Winnipeg, Manitoba, Canada R3T 2N2*
[2]*Department of Physics, Princeton University, Princeton, New Jersey 09054*
[3]*Exxon Research and Engineering Company, Route 22 East, Annandale, New Jersey 08801*
(Received 6 April 1995)

We have critically tested the application of the diffusion approximation to describe the propagation of ultrasonic waves through a random, strongly scattering medium. The transmission of short ultrasonic pulses has been measured through a concentrated suspension of glass beads immersed in water. The transmitted sound field is found to exhibit temporal fluctuations with a period determined by the width of the incident pulse. Provided that appropriate boundary conditions are used to account for the reflectivity of the interfaces, the time dependence of the ensemble-averaged transmitted intensity is shown to be well described by the diffusion equation. This enables us to determine both the diffusion coefficient for the sound waves as well as the inelastic absorption rate. The consistency of these results is established by varying the experimental geometry; while the transmitted pulse shape changes markedly, the values for the diffusion coefficient and absorption rate obtained through a description using the diffusion approximation remain unchanged. We have also measured the absolute transmitted intensity of the sound as the sample thickness is varied; this provides an accurate measure of the transport mean free path and thus also the energy transport velocity. These results convincingly demonstrate the validity of using the diffusion approximation to describe the propagation of sound waves through strongly scattering media.

PACS number(s): 43.35.+d, 43.20.+g, 62.30.+d

I. INTRODUCTION

The description of the propagation of classical waves through strongly scattering media is a problem of considerable importance to many areas of physics [1]; it is also a problem of great difficulty and a full understanding has as yet remained elusive, despite considerable research effort. However, much progress has been achieved in recent years through the study of the propagation of electromagnetic waves through strongly scattering materials [1]. To a considerable extent, this progress has been based on the success of the diffusion approximation in describing the propagation. Within this picture, the phase information of the scattering processes is neglected and the propagation of the average energy density is approximated as a diffusive process. The diffusion coefficient is $D = v_e l^*/3$, where the transport mean free path l^* is the mean distance traveled before the direction of propagation is randomized and v_e is the velocity at which the energy is transported. The solution of the diffusion equation determines the distribution of multiple scattering paths; each of these paths is then assigned a phase based on its total length. This approach has been particularly successful with electromagnetic waves, including light and microwaves; it correctly accounts for a wide variety of fascinating phenomena, from the enhancement of the backscattered radiation [2,3] to the correlations of the transmitted intensity with variations in the incident frequency [4], the angle of the sample [5], or the temporal position of the scatterers [6,7].

While this approach has been very successfully and widely applied to electromagnetic waves, the essential physics of the approximation is completely general to all types of classical waves. Thus it should apply equally well to the description of the propagation of acoustic waves. This could be of considerable practical importance; the measurement of the velocity and attenuation of sound waves provides a sensitive probe of both the structure and the properties of the material through which they propagate. Virtually all standard ultrasonic measurements focus on the use of ballistically propagating, or unscattered, sound. However, many materials and media of technological interest scatter sound very strongly, providing an important practical impetus for exploring the extension of the use of the diffusion approximation to the description of the propagation of sound waves. Furthermore, the underlying physics of diffusing sound may differ in unexpected but significant ways from that of electromagnetic waves, thereby adding considerable richness to the description of the phenomena. For example, the presence of transverse waves in solid scatterers may lead to interesting new effects. In addition, the impedance mismatch of scattering particles can easily be made significantly larger for sound than for light; this may facilitate the observation of disorder-induced localization effects of a classical wave. However, to date, there have been few investigations of the application of the diffusion approximation to the description of the propagation of sound waves through strongly scattering media [8–10] and the applicability of the full diffusion treatment to sound has not been critically tested. In this paper, we study the application of the diffusion approximation to the propagation of ultrasound pulses transmitted through glass beads in water. We exploit the considerable knowledge of diffusive propagation gained from the study of light to provide a detailed description of the

behavior of multiply scattered sound waves; this enables us to critically test the applicability of the diffusion approximation for sound. We show that the diffusion approximation does indeed provide an excellent description of the propagation and we measure the key parameters essential for the application of this model.

In our experiments, we have investigated the propagation of ultrasonic pulses through slabs of strongly scattering glass beads immersed in water. Using a very small detector, we have measured the amplitude of the scattered sound in a single coherence area, or speckle spot; this exhibits a rapidly fluctuating and highly dispersive character. To compare to the diffusion equation, which describes the propagation of the average intensity, we have determined the scattered intensity of the sound from the amplitude measurements and performed an ensemble average over a large number of speckles. This allows us to measure the pulse shape of the average multiply scattered intensity that is transmitted through the medium and to compare these data to the shape predicted by the diffusion equation. By studying samples of different thicknesses, we show that excellent agreement can be obtained only if the effects of the boundaries are properly accounted for in a fashion analogous to the methods developed for describing the diffusive propagation of light [5,11]. The description of the pulse shape provides a measure of the diffusion coefficient D of the sound as well as the inelastic absorption time τ_a. The consistency of this description is confirmed by comparing the results obtained using a focused and an expanded incident beam; these different geometries significantly modify the shape of the transmitted pulse but yield identical values of both D and τ_a. A further consistency check is obtained in the point source geometry by measuring the ratio of the off-axis to the on-axis intensity; this ratio gives an independent measure of D that is not complicated by boundary and absorption effects and gives a value that is in excellent agreement with the analysis of the on-axis pulse shape. We have also measured the absolute transmission of the sound in a quasi-continuous-wave configuration, allowing us to determine the transport mean free path l^* of the diffusing sound from the dependence of the absolute transmission on the sample thickness. From these two separate measurements of D and l^*, we are able to determine the velocity of energy transport v_e for the diffusing sound. This is the first reported measurement of either l^* or v_e for diffusive sound. Our results unambiguously establish the validity of the diffusion approximation for multiply scattered sound.

II. EXPERIMENT

The propagation of very strongly scattered sound waves was studied using samples consisting of glass beads immersed in water, for which the acoustic impedance ratio is approximately 10. The scattering was further enhanced by choosing the glass bead diameter to be the same order of magnitude as the acoustic wavelength in water. This was accomplished by performing the experiments at an ultrasonic frequency of 2.5 MHz and using beads with a radius a of 0.5 mm. The glass beads were contained in disk-shaped cells having thin, parallel polystyrene walls glued to a uniform spacer ring; this ring formed the outer circumference of the disk and had a diameter that was at least ten times larger than the cell thickness. The beads were relatively uniform in size and were carefully packed into the water-filled sample cells so as to avoid trapped air bubbles, which would have caused significant additional ultrasonic absorption, obscuring the propagation of the multiply scattered sound. The beads were packed at a volume fraction near the limit of random close packing, or about 63%.

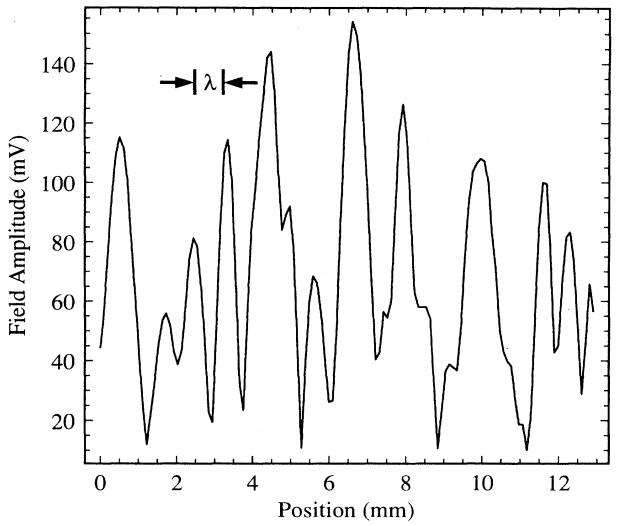

FIG. 1. Cross section of the acoustic speckle pattern of multiply scattered sound transmitted through a 20-mm-thick sample containing 0.5-mm-radius glass beads immersed in water. The speckle pattern was detected in the near field. The coherence area is approximately λ^2, where $\lambda = 0.6$ mm is the ultrasonic wavelength in water.

One of the experimental challenges in measuring multiply scattered ultrasonic radiation arises from the rapid spatial fluctuations that occur in the phase and amplitude of the scattered sound at the detecting plane. These fluctuations are caused by the interference between the ultrasonic waves that have traveled different paths through the sample, resulting in acoustic speckles that are analogous to the more familiar case of optical speckles. Since piezoelectric transducers measure the average acoustic *field* across the surface of the detector, these rapid spatial fluctuations give rise to spurious phase cancellation effects when conventional large-diameter transducers are used as detectors, leading to grossly inaccurate results. To overcome this serious experimental limitation, we have used a miniature hydrophone, whose diameter is much less than the ultrasonic wavelength, to detect the scattered radiation over a single coherence area. We illustrate these spatial fluctuations in Fig. 1, where we show a typical example of the near-field acoustic speckle pattern of the multiply scattered sound exiting one of our glass bead samples. These data were collected by scanning the small hydrophone across the face of the sample.

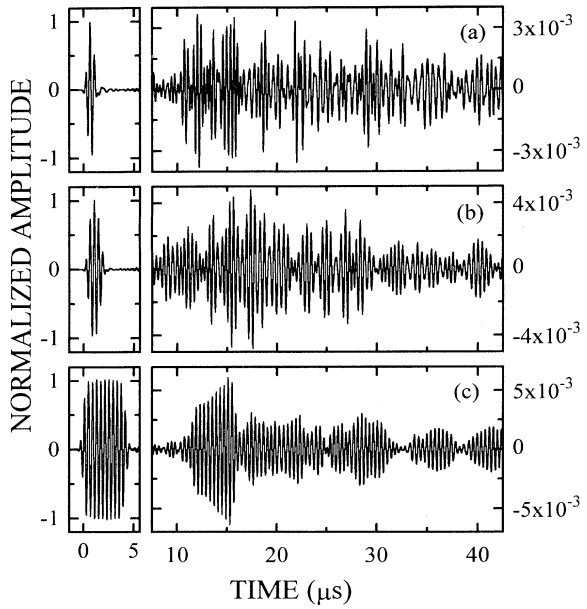

FIG. 2. Time evolution of the transmitted ultrasonic fields in a single speckle (right) for three different incident pulse widths (left), showing the temporal fluctuations of the multiply scattered fields.

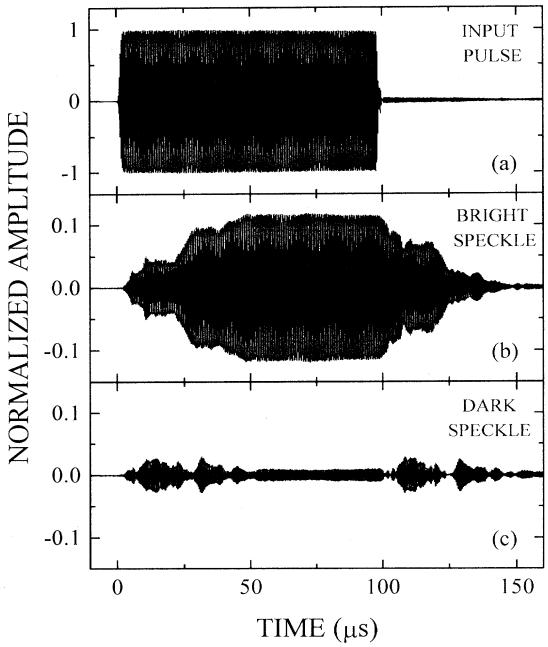

FIG. 3. Transmitted ultrasonic field in a single speckle for an incident pulse width of 100 μs. The incident pulse is shown in (a) and the transmitted fields in typical bright and dark speckles are shown in (b) and (c). Note the region from about 60 to 100 μs, where the amplitude is essentially flat, corresponding to the quasi-continuous-wave case in which the entire distribution of allowed path lengths are filled.

They confirm that the width of the coherence area over which the ultrasonic signal is essentially constant is approximately equal to the ultrasonic wavelength λ. Thus the use of the miniature hydrophone successfully eliminates the deleterious effects of having more than a single speckle impinge on the detector, while retaining the excellent sensitivity of ceramic piezoelectric transducers, thereby making measurements of multiply scattered ultrasound feasible.

The experiments were performed in a water tank, which provided a convenient coupling medium between the transducers and the sample cell and allowed their relative positions to be readily varied. Two different experimental geometries were employed. In the first, we used a point-source geometry, in which an incident sound pulse was generated by a focusing transducer arranged so that its focal plane was coincident with the face of the sample closest to the transducer. The miniature detecting hydrophone was placed near the opposite face of the sample, on axis with the generating transducer. Signals from statistically independent ensembles of the glass-bead disorder were collected by translating the sample. A second experimental geometry was used to obtain a good approximation to a plane-wave source; here the sample was placed in the far field of a 6-mm-diam generating transducer, thereby ensuring a uniform illumination of the front face of the sample. For the plane-wave experiments, the sample was fixed in position and the detector scanned over the central portion of the back face of the sample cell to collect the transmitted sound in many speckles. The signal-to-noise ratio of the detected wave forms was improved by averaging the detected signals for each speckle using a digitizing oscilloscope.

The experiments were performed using different input pulse widths, ranging from very short pulses that have widths less than 1 μs to very long pulses that are a good approximation to continuous waves. An example of the signal detected in a single coherence area for a short pulse transmitted through a 10-mm-thick sample cell containing 0.5-mm-radius beads is shown in Fig. 2(a). The incident pulse consisted of only two oscillations centered at a frequency $f=2.45$ MHz and is shown to the left. By contrast, multiple scattering in the sample causes the transmitted signal to be spread out over a time interval exceeding 70 μs as the sound that has traveled progressively longer and longer paths reaches the detector. The transmitted pulse also exhibits large temporal fluctuations that modulate the more rapid carrier frequency oscillations at $f\approx 2.45$ MHz. These fluctuations of the wave-form envelope have a characteristic period that represents the time over which the magnitude and phase of the detected field remain essentially unchanged and is of the order of the input pulse width. Physically this reflects the fact that the maximum overlap of the paths contributing at any time is determined by the width of the incident pulse, so that as the incident pulse width is increased, the characteristic width of these temporal fluctuations also increases proportionally. This is illustrated by Figs. 2(b) and 2(c), which show the signal transmitted through the same sample when the pulse width is increased first to about four oscillations [Fig. 2(b)] and then

to about ten oscillations [Fig. 2(c)]. In both cases, the temporal fluctuations of the envelope vary on a time scale that corresponds to the greater input pulse widths. These temporal fluctuations are a consequence of the interference effects of the sound transmitted along different paths. Unlike the case for light, these interference effects can be directly measured using sound because *both* the amplitude and the phase of the scattered waves are detected.

As a final illustration of the interference effects associated with different samplings of the path distributions in the sample, we show in Fig. 3 the effect of increasing the incident pulse width to 100 μs, a time interval that exceeds the longest transit times for the scattered sound to travel through the sample. This incident pulse is shown in Fig. 3(a), normalized for comparison with the transmitted signals to an amplitude of ± 1. Figures 3(b) and 3(c) show the relative amplitudes of the signals transmitted through a 10-mm-thick glass bead sample. The data in Figs. 3(b) and 3(c) were taken for two different positions of the detector, corresponding to bright and dark speckles, respectively. Fluctuations in the transmitted signals are still observed during the first 50–60 μs, whereupon the entire distribution of different path lengths become simultaneously "filled" and the signal level becomes constant, as would be expected for continuous-wave transmission. Unlike the continuous-wave situation, however, this plateau lasts only until the end of the input pulse, after which rapid fluctuations are again observed as the occupation of the path distributions for these particular ensembles of scatters decays away. The time interval over which these fluctuations persist is similar to the time for the sound to diffuse through the sample in the short pulse experiments, again showing the temporal interference effects that are directly observable in ultrasonic experiments.

III. RESULTS

To ascertain the validity of the diffusion approximation in describing the sound propagation, we first determined the time dependence of the average intensity of the transmitted pulse in the point source geometry with the detector transducer on axis with the source transducer. We used an input pulse containing about ten oscillations, as shown in Fig. 2(c), so that the frequency is reasonably well defined. We measured the ultrasonic field over N independent coherence areas by translating the sample while keeping both transducers fixed. To ensure that independent coherence areas are probed, the sample was moved between each measurement a distance equal to at least the sample thickness. The envelope of the square of each individual wave form was then determined from the maximum of each cycle in the transmitted pulse; the resulting signal, which is proportional to the transmitted intensity, was ensemble averaged over all N speckles. The data were normalized by dividing the signal by the measured intensity of the incident pulse. Typical results of this ensemble average, measured for $N \approx 85$ and an incident pulse width of 4.2 μs, are shown in Fig. 4 for three different sample thicknesses. The results exhibit the characteristic shapes of diffusively transmitted pulses;

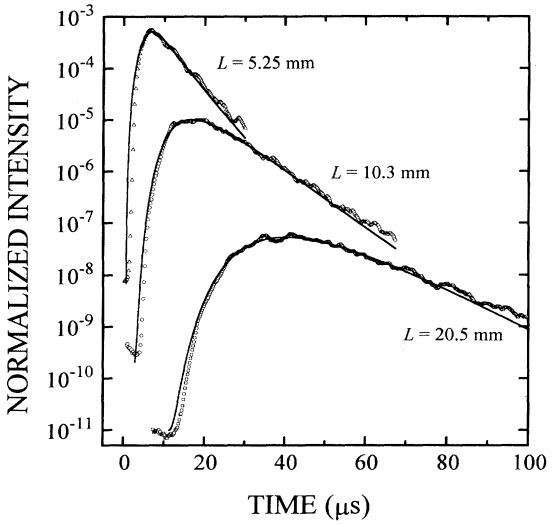

FIG. 4. Time profile of the average intensity transmitted through randomly close-packed suspensions of glass beads for three sample thicknesses L. The smooth solid curves are the best least-squares fits to diffusion theory, giving $D = 0.43 \pm 0.02$ mm$^2/\mu$s and $\tau_a = 12 \pm 1$ μs.

they are plotted on a logarithmic scale to accommodate the large changes that are observed in the transmitted intensity as the sample thickness is varied. As the sample thickness is increased, not only does the overall intensity decrease dramatically, but the pulse broadens and the peak occurs at later times. For all these data, the magnitude of the temporal fluctuations that remain after ensemble averaging the transmitted intensity is of order $\sqrt{N}$, consistent with averaging independent speckles.

To describe the diffusive nature of the sound propagation, we compare the measured pulse shape of the average scattered intensity to that determined by calculating the transmitted flux using the solution of the diffusion equation for the acoustic energy density $U(x,y,z)$ in a slab of thickness L having infinite transverse extent [12]. To account for the initial conditions, the incident sound is assumed to be a δ function in time and position, which begins to diffuse after traveling a distance z_0 into the sample. To account for the boundary conditions, we assume that no diffusing flux is incident into the sample at the faces apart from a contribution due to internal reflections [5,11]. For these boundary conditions, the transmitted flux $J(t)$ normal to the slab is given by

$$J(t) = -D \frac{\partial U}{\partial z}\bigg|_{z=L}$$

$$= \frac{e^{-r^2/4Dt} e^{-t/\tau_a}}{2\pi L^2 t} \sum_{n=1}^{\infty} A_n e^{-D\beta_n^2 t/L^2}, \qquad (1)$$

with

$$A_n = \frac{\beta_n[\beta_n K \sin\beta_n - \cos\beta_n][\sin(\beta_n z_0/L) + \beta_n K \cos(\beta_n z_0/L)]}{\beta_n^2 K^2 + 1 + 2K} . \quad (2)$$

Here the values of β_n are given by the zeros of the equation

$$\tan\beta = \frac{2\beta K}{\beta^2 K^2 - 1} \quad (3)$$

and the dimensionless constant K is given by

$$K = \frac{2l^*}{3L}\frac{1+R}{1-R} . \quad (4)$$

The calculated reflectivity $R(\theta)$ of the cell walls is averaged over the incident angles θ [5] to obtain $R = 0.24$. We allow for the possibility that the detector is positioned a distance $r = \sqrt{(x-x_0)^2 + (y-y_0)^2}$ from the axis of the source centered at (x_0, y_0) and integrate Eq. (1) over the width of the detector. Finally, to account for the finite width of the incident pulse, we also convolute Eq. (1) with the incident pulse shape, and to account for uncertainty in the normalization of the input pulse, we multiply Eq. (1) by an adjustable constant that is always found to be of order unity in the fit.

The time profile of the average transmitted intensity depends sensitively on both the diffusion coefficient and the absorption time; the initial rise of the pulse is determined by D, while the decay is strongly influenced by τ_a. The decay is also influenced by the cell wall reflectivity R since large values of R have the effect of lengthening the diffusive pulse by causing sound to remain longer in the sample. However, the fitted parameters D and τ_a are only weakly dependent on R for the range of sample thicknesses investigated and it would be necessary to vary R by more than a factor of 2 from its calculated value to have a significant effect on the determination of these parameters from our data. Thus R was held constant at its calculated value of 0.24 while fitting our data. We expect the effects of the penetration depth z_0 to be small in thick samples, where the dominance of long diffusion path lengths through the sample will make the data relatively insensitive to z_0; by contrast, the results for the thin samples should show a strong dependence on z_0. However, the values of D and τ_a should be completely independent of thickness. We therefore fit the data for each thickness in Eq. (1) using different values of z_0 and plot the values of D and τ_a obtained in these fits as shown in Figs. 5(a) and 5(b), respectively. As expected, the results of the thinnest sample are relatively sensitive to the value of z_0 used in the fit, while the results for the thicker samples are much less sensitive. We find a reasonably narrow range of values for z_0, between about 0.7 and 1 mm, where consistent values of D and τ_a are found for the three thicknesses. These self-consistent fits yield $D = 0.43 \pm 0.02$ mm$^2/\mu$s and $\tau_a = 12 \pm 1$ μs. Moreover, if we assume that $z_0 = l^*$, as predicted by computer simulations [13], we obtain an estimate for the transport mean free path of $l^* \approx 0.85 \pm 0.2$ mm. As shown by the solid lines in Fig. 4, an excellent fit to the data for all three thicknesses is obtained using these values.

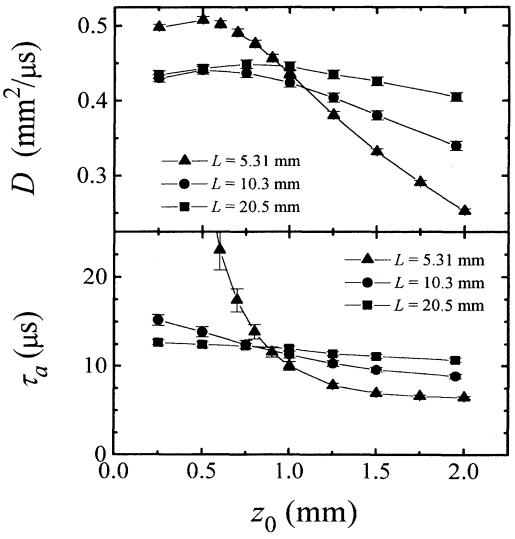

FIG. 5. Dependence of the fitted parameters D and τ_a on the penetration depth z_0 for the data shown in Fig. 4. The consistency of the fitted parameters for z_0 between 0.7 and 1 mm gives an estimate for l^* of 0.85 ± 0.2 mm.

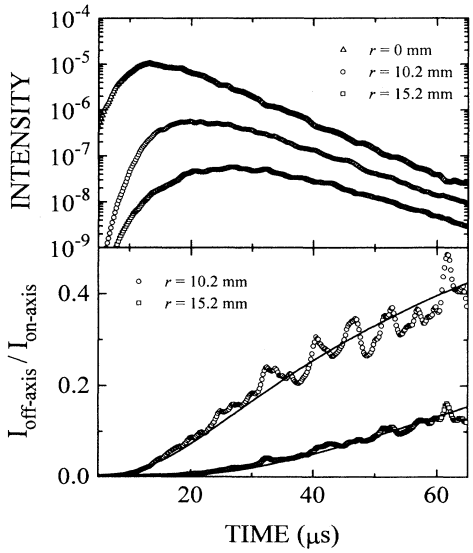

FIG. 6. Comparison of the transmitted intensity $I(t)$ measured with the detector displaced a distance r away from the axis of the source to that measured with the detector placed directly on axis. The solid curves in the lower panel show the expected exponential reduction in the ratio of off-axis to on-axis intensity and give a measure of D that is independent of absorption and boundary effects.

As a further confirmation of the accuracy of our determination of D and of the consistency of the description using the diffusion approximation, we exploit the use of a point source and a point detector. If we move the detector a distance r away from the axis of the source, the transmitted intensity is decreased by $\exp(-r^2/4Dt)$, independent of all other variables. The reason for this is that the pulses arriving at the same time for each position of the detector must follow paths of the same length; however, fewer paths contribute to the off-axis detector, thus reducing the signal. This is independent of absorption, and hence τ_a, and is independent of boundary effects, and hence z_0 and R. We show typical results in Fig. 6, where we compare, in the upper panel, the time dependence of the average intensity measured with the detector on axis to the intensity that is measured when the detector is displaced 10.2 mm off axis (middle set of points) and 15.2 mm off axis (lowest set of points). In the lower panel, we plot the ratio of the average intensity for the two off-axis positions to that obtained with the detector on axis. The data are significantly different; far fewer paths reach the detector when it is further off axis and the ratio is correspondingly lower. However, both sets of data for the intensity ratios are well described by the predicted exponential form, as shown by the smooth lines through the data in Fig. 6. In obtaining these fits, the finite spatial width of the input beam and the detector must be accounted for; this is accomplished by convoluting the exponential expression with the measured spatial profile of the incident beam and with the detector area. From this behavior, we obtain values of D of 0.44 ± 0.03 $\text{mm}^2/\mu\text{s}$ for the detector placed 10.2 mm off axis and 0.46 ± 0.03 $\text{mm}^2/\mu\text{s}$ for the detector placed 15.2 mm off axis, in excellent agreement with the value obtained by fitting Eq. (1) to the on-axis data.

As an additional check of the applicability of the diffusion approximation, we measure the shape of the transmitted intensity pulse for a different geometry, using a plane-wave source. We expect the shape of the diffusive pulse to differ noticeably; however, the values of the parameters should remain unchanged if the diffusion approximation is valid. We compare data obtained using a plane-wave source and a point source, for the same sample with $L=10.2$ mm, in Fig. 7. The transmitted pulse measured with the plane-wave source is noticeably longer than that obtained with the focused source and reaches its peak value at a later time. This reflects the larger contribution of sound waves traveling over longer paths from the plane-wave source. To fit the plane-wave data, we integrate x_0 and y_0 in Eq. (1) over the input face of the slab to obtain

$$J(t)=\frac{2D}{L^2}e^{-t/\tau_a}\sum_{n=1}^{\infty}A_n e^{-D\beta_n^2 t/L^2}, \tag{5}$$

where A_n, β_n, and K are again given by Eqs. (2)–(4). This differs from Eq. (1) for an on-axis point source only by the multiplicative factor $4\pi Dt$, thus predicting that the ratio of the plane-wave to point source time profiles increases linearly with time. We find that the linear time dependence of this ratio is indeed well obeyed by our data, again confirming the validity of the diffusion approximation, although the normalization of the point source data is too uncertain to use the slope to obtain a precise estimate of D. However, D can be determined by fitting Eq. (5) directly to the plane-wave data. The smooth line through the data obtained with the plane-wave source, shown in Fig. 7, is the fit with $z_0=0.85$ mm and provides an excellent description of the time dependence of the data. From this fit, we obtain $D=0.43\pm0.02$ $\text{mm}^2/\mu\text{s}$ and $\tau_a=11\pm1$ μs; these values are in good agreement with the values obtained from the fit for the focused geometry. This confirms the robustness of the fit and the applicability of the diffusion approximation to the description of the propagation.

The absorption rate τ_a^{-1} is surprisingly large, being much greater than expected for either water or pure glass. To investigate the origin of this large absorption, we repeated the measurements using a different bead size, with $a=0.25$ mm. Surprisingly, we find that the absorption rate is independent of a. Thus the absorption cannot be due to the usual viscous losses encountered in a fluid near a fluid-solid interface, even though these losses might be expected to be significant because of the large interfacial area in our glass bead sample. However, this mechanism [14] gives an absorption rate proportional to the surface area and hence, for close-packed spheres, to a^{-1}, which is not observed. Instead, it appears that the absorption is intrinsic to the glass beads themselves, as the measured absorption depends solely on the amount of glass in the suspension and presumably results from the method by which the spheres are manufactured.

An additional critical parameter in the diffusion approximation is the transport mean free path l^*. While we obtain an estimate of l^* from the value of z_0 that provides the best fit to the pulse shape data, a far more accurate value can be obtained by measuring the absolute transmission. However, to correctly account for all the boundary and absorption effects, this must be done as a

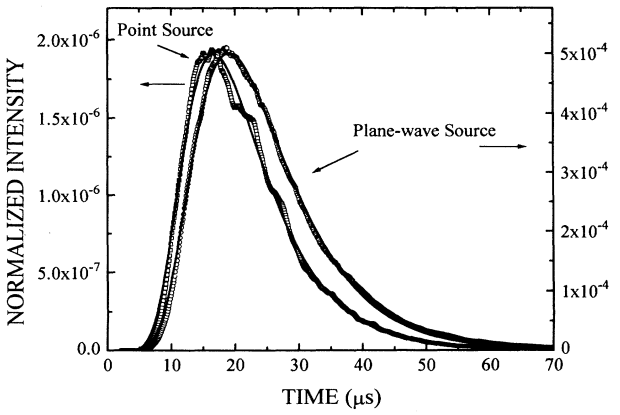

FIG. 7. Comparison of the time profile of the transmitted intensity for a point source and a plane-wave source. The smooth solid curves are fits to the corresponding expressions given by diffusion theory and provide another check of the applicability of the diffusion approximation.

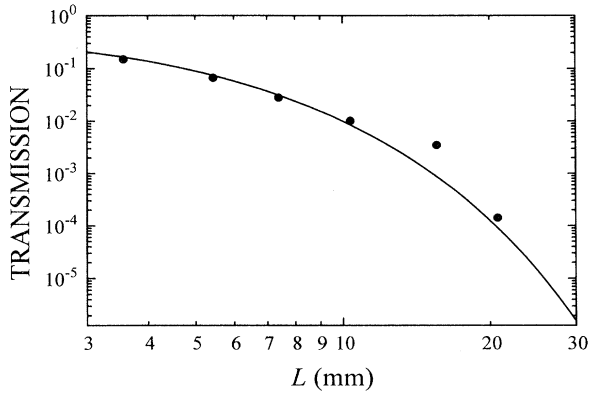

FIG. 8. Dependence of the absolute transmission on sample thickness L. The incident ultrasonic beam was generated using the plane-wave geometry with a sufficiently long pulse that continuous-wave conditions were obtained to an excellent approximation. The fit to Eqs. (6) and (7), shown by the solid curve, gives $l^*=0.8\pm0.05$ mm.

function of sample thickness. This is most accurately accomplished using a plane-wave source, so that the transmitted intensity is independent of the position of the detector. The theoretical description of the total transmitted intensity is most readily determined for continuous-wave conditions; thus, to approximate these, we used very broad input pulses, of about 100 μs in length. As shown in Fig. 3, this ensures that virtually all the paths are excited during the middle portion of the pulse, so that, during this interval, the transmitted intensity is constant in time. We again average the intensity over about 100 independent speckles; in this case the averaging is accomplished by squaring the measured fields of each speckle and averaging these over the flat central portion of the pulse to obtain a value for the average transmitted intensity for each speckle. Since the sample is illuminated nearly uniformly, the detector is translated over the central region to collect data from different speckles. To obtain a measure of the absolute transmitted intensity, data are collected with the sample removed and the ratio is determined. Since this is an absolute measure of the transmitted intensity, great care must be taken to obtain accurate data. Thus we measure the intensity profile of the incident beam without the sample and average over this to account for the small inhomogeneities in its spatial profile. We also normalize the transmission measurement for each speckle by the incident power measured concurrently to eliminate the effects of any drifts in the input power. Finally, we account for the effects of the sample cell walls by repeating the measurement using a sample to which a polyacrylimide gel had been added; this allows the cell walls to be removed while still maintaining the shape of the sample slab. Following these procedures, we are able to obtain reasonably accurate measures of the absolute transmission.

The data obtained as the sample thickness is varied are plotted logarithmically in Fig. 8. To account for the thickness dependence of the transmission, we compare these data to [13]

$$T=\frac{\left[1+\frac{KL}{l^*}\right]-\left[1+\frac{KL}{l^*}+\frac{L}{l^*}\right]e^{-L/l_s}}{\left[\frac{L}{l^*}+\frac{2KL}{l^*}\right]}g_1(\tau_a)\ , \tag{6}$$

where the second term in the numerator contributes only for the thinnest samples and accounts for the small contribution of the unscattered sound. The scattering mean free path l_s is determined by an independent measurement of the ballistic transmission. This is performed using large area transducers, which are relatively insensitive to the diffusive sound because of the phase cancellation of the independent speckles, but are better able to detect the weak ballistic transmission. We measure a value of $l_s=0.75$ mm. We must also account both for the effects of absorption and for the experimental boundary conditions, the latter being the same as in the pulse propagation experiments. This can be accomplished most directly by using the angular correlation function for diffusing light in the presence of absorption, which has been determined for this geometry and with these boundary conditions [5]. We evaluate it at zero angle and obtain

$$g_1(\tau_a)=\frac{\left[\frac{L+2KL}{z_0+KL}\right]\left\{\sinh\left[z_0\left[\frac{1}{D\tau_a}\right]^{1/2}\right]+KL\left[\frac{1}{D\tau_a}\right]^{1/2}\cosh\left[z_0\left[\frac{1}{D\tau_a}\right]^{1/2}\right]\right\}}{\left[1+\frac{K^2L^2}{D\tau_a}\right]\sinh\left[L\left[\frac{1}{D\tau_a}\right]^{1/2}\right]+2KL\left[\frac{1}{D\tau_a}\right]^{1/2}\cosh\left[L\left[\frac{1}{D\tau_a}\right]^{1/2}\right]}\ . \tag{7}$$

The solid line in Fig. 8 is a plot of the theoretical predictions of Eqs. (6) and (7) using the values of D and τ_a determined from the pulse experiments (Fig. 4) and a value of $l^*=z_0=0.8$ mm. The agreement with the data is quite good, except for one of the thicker samples where the transmission is greatly reduced and the data are less reliable. In fact, for $L>10$ mm, several factors conspire to reduce the accuracy of the experimental results. As the sample thickness increases, we are unable to enlarge the illuminating beam proportionately, so that, for the two thickest samples, the incident beam is no longer as good an approximation to a plane wave. Also, for these

samples, it becomes difficult to fill all of the paths simultaneously using a 100-μs-wide pulse, so that the continuous-wave approximation begins to break down. A third factor is the severe reduction in the signal-to-noise ratio for the thickest samples, causing increased scatter in the data. However, for the thinner samples, the data are of excellent quality and the agreement between the data and the theory is sufficiently good that we estimate the uncertainty in l^* to be no more than ± 0.05 mm. This represents a rather good determination of the transport mean free path.

Finally, we can also determine the energy transport velocity for the diffusing sound from our measurements of D and l^*, using $v_e = 3D/l^*$. We obtain $v_e = 1.6 \pm 0.1$ km/s. Interestingly, this value is very close to the velocity of ballistic propagation, which we measure to be 1.7 ± 0.1 km/s from the transit time of the weak unscattered pulse that was detected in the scattering mean free path measurement. It is also interesting to compare the energy velocity with the speed of sound in water, which is 1.5 km/s, and with the longitudinal and transverse sound speeds in the glass, which are 5.7 and 3.4 km/s, respectively. Thus the energy transport velocity is only slightly faster than the speed of sound in pure water and is much slower than the sound speeds in glass. This relatively slow velocity compares favorably with the behavior observed with light, where the energy transport velocity can be slowed significantly because of scattering resonances [15,16].

IV. CONCLUSIONS

In this paper we have shown that the propagation of sound waves through very strongly scattering media can be well described by means of the diffusion approximation. In this regard, sound behaves in a manner analogous to another classical wave, light, and we are able to exploit much of the recent knowledge gained from the study of diffusing light waves to accurately account for the behavior of diffusing sound. We have measured the propagation of short pulses of sound through a sample consisting of glass beads immersed in water. Very strong scattering was ensured by using beads that are comparable in size to the wavelength of the sound in the water. We have used a very small detecting transducer to probe the scattered sound field within a single spatial coherence area. The amplitude of the transmitted pulse is observed to fluctuate in time with a period roughly set by the length of the incident pulse. The ensemble average of the transmitted intensity was determined by averaging over many independent coherence areas, allowing the pulse shape to be measured. This is found to be much longer than the incident pulse, reflecting the long path lengths traveled by the multiply scattered sound waves. The time dependence of the average transmitted intensity is very well described by the diffusion approximation, provided that appropriate boundary conditions are used, which account for the reflectivity of the interfaces. From a fit to the transmitted pulse shape for different sample thicknesses, we are able to determine both the diffusion coefficient for the sound and the absorption rate. The validity of the diffusion approximation is further established by repeating these measurements using a different geometry; the pulse shape is changed, but it is still well described by the diffusion approximation for the new geometry, using the same values for the coefficients. Finally, we also measure the absolute transmitted intensity as the sample thickness is varied. We again account for the observed behavior within the diffusion approximation using the same boundary conditions. This enables us to accurately determine the transport mean free path of the diffusing sound waves. Combining this measure of the transport mean free path with the measure of the diffusion coefficient obtained from the pulse shape data, we are able to determine the energy transport velocity.

Our results provide a critical test of the applicability of the diffusion approximation to the description of sound propagating through a multiply scattering medium and we conclude that this description is highly accurate. Unlike light, the use of sound has the distinct advantage that the full field amplitude can be simply detected, including all the phase information. This additional phase information has not yet been included in any theoretical treatments of the diffusive propagation of classical waves; doing so will help account for the data available with sound measurements and may provide new insights into the nature of the propagation. Moreover, this phase information will allow additional measurements to be made; for example, the dynamics of the medium might be probed using the acoustic equivalent of diffusing-wave spectroscopy [6,7]. In addition, using scatterers with significantly less intrinsic absorption, but with significantly larger scattering cross sections, may facilitate the observation of nonclassical propagation effects, such as scale-dependent diffusion coefficients, that are a signature of the localization of sound. Thus the results presented here open up interesting possibilities for using acoustic techniques in future studies of the propagation of multiply scattered classical waves, thereby transcending some of the limitations inherent in light scattering experiments.

ACKNOWLEDGMENTS

We gratefully acknowledge valuable discussions with Ping Sheng. This work was supported by NSERC of Canada and by a NATO collaborative research grant.

[1] *Scattering and Localization of Classical Waves in Random Media,* edited by P. Sheng (World Scientific, Singapore, 1990).

[2] M. P. van Albada and A. Lagendijk, Phys. Rev. Lett. **55**, 2692 (1985).

[3] P. E. Wolf and G. Maret, Phys. Rev. Lett. **55**, 2696 (1985).

[4] J. M. Drake and A. Z. Genack, Phys. Rev. Lett. **63**, 259 (1989).

[5] J. X. Zhu, D. J. Pine, and D. A. Weitz, Phys. Rev. A **44**, 3948 (1991).

[6] G. Maret and P. E. Wolf, Z. Phys. B **65**, 409 (1987).
[7] D. J. Pine, D. A. Weitz, P. M. Chaikin, and E. Herbolzheimer, Phys. Rev. Lett. **60**, 1134 (1988).
[8] H. M. Jaeger and S. R. Nagel, Science **225**, 1523 (1992).
[9] G. Bayer and T. Niederdrank, Phys. Rev. Lett. **70**, 3384 (1993).
[10] R. L. Weaver and W. Sachse (unpublished).
[11] A. Lagendijk, R. Vreeker, and P. De Vries, Phys. Lett. A **136**, 81 (1989).
[12] H. S. Carslaw and J. C. Jaeger, *Conduction of Heat in Solids* (Clarendon, Oxford, 1990).
[13] D. J. Durian, Phys. Rev. E **50**, 857 (1994).
[14] L. D. Landau and E. M. Lifshitz, *Fluid Mechanics* (Pergamon, Oxford, 1959).
[15] B. A. van Tiggelen, A. Lagendijk, M. P. van Albada, and A. Tip, Phys. Rev. B **45**, 12 233 (1992).
[16] C. M. Soukoulis, S. Datta, and E.N. Economou, Phys. Rev. B **49**, 3800 (1994).